Research Article

Cancer Immunology Research

Immunosuppressive Immature Myeloid Cell Generation Is Controlled by Glutamine Metabolism in Human Cancer

Wen-Chao Wu[1], Hong-Wei Sun[1], Jing Chen[1,2], Han-Yue OuYang[1], Xing-Juan Yu[1], Hai-Tian Chen[3], Ze-Yu Shuang[1], Ming Shi[1], Zilian Wang[3], and Limin Zheng[1,2]

Abstract

Tumor-associated myeloid cells are one of the prominent components of solid tumors, serving as major immune regulators for the tumor microenvironment (TME) and an obstacle for immune-checkpoint blocking (ICB) therapy. However, it remains unclear how metabolic processes regulate the generation of suppressive myeloid cells in the TME. Here, we found that hematopoietic precursor cells are enriched in the tissues of several types of human cancer and can differentiate into immature myeloid cells (IMC). Tumor-infiltrating IMCs are highly immunosuppressive, glycolytic, and proliferative, as indicated by high levels of M-CSFR, Glut1, and Ki67. To elucidate the role of metabolism in regulating the generation of IMCs, we induced suppressive IMCs from hematopoietic precursor cells with GM-CSF and G-CSF *in vitro*. We found that the generation of suppressive IMCs was accompanied by increased glycolysis, but not affected by glucose deprivation due to alternative catabolism. Generation of IMCs relied on glutaminolysis, regardless of glucose availability. Glutamine metabolism not only supported the expansion of IMCs with glutamine-derived α-ketoglutarate but also regulated the suppressive capacity through the glutamate–NMDA receptor axis. Moreover, inhibition of glutaminase GLS1 enhanced the therapeutic efficacy of anti–PD-L1 treatment, with reduced arginase 1^+ myeloid cells, increased $CD8^+$, $IFN\gamma^+$ and granzyme B^+ T cells, and delayed tumor growth in an ICB-resistant mouse model. Our work identified a novel regulatory mechanism of glutamine metabolism in controlling the generation of suppressive IMCs in the TME.

Introduction

Tumor-associated myeloid cells are a group of heterogeneous myeloid cells that have emerged as one of the predominant regulators of immune response in cancer (1–3). These myeloid cells can enhance cancer cell stemness (4), support angiogenesis and metastasis (5), and promote resistance to chemotherapy, radiotherapy, and immune-checkpoint blocking (ICB) therapy (6–8). Immunosuppressive myeloid cells are generated in the bone marrow from myeloid progenitor cells (9), and then recruited by tumor tissues. Hematopoietic progenitor cells (HPC) can be directly recruited and accumulated in peripheral tissues, where they serve as an important source of descendant cells (10, 11). However, we know little about how these infiltrating HPCs differentiate into functional myeloid cells in the tumor microenvironment (TME).

Growing evidence indicates that the metabolism of a cell can have a marked impact on its function (12). For example, high blood glucose levels in type 2 diabetes cause endothelial cells to increase fatty acid oxidation (FAO), subsequently promoting atherosclerosis and microangiopathy (12, 13). Activated T cells require upregulation of glucose and amino acid catabolism for rapid proliferation and cytokine production (14). On the other hand, polarization of macrophages from M1 to M2 is regulated by the switch from glycolysis to lipid metabolism and oxidative phosphorylation (OxPhos; refs. 15, 16). These observations suggest that the metabolism of cells determines their differentiation and function, potentially offering therapeutic insight.

Nutrient-limiting TME can metabolically reprogram infiltrating immune cells and propagate immune escape (17). Glucose and nutrient deficiency in the TME impairs T-cell receptor signaling in activated T cells, resulting in anergy and exhaustion (18, 19). Notably, some immunosuppressive cells, such as regulatory T cells (Treg) and macrophages, can alter their metabolic pathway to adapt to TME (20, 21). They have low glycolysis rates, but sustain high mitochondrial biogenesis, relying on FAO to exert their immunosuppressive effect (22, 23). However, little is known about how the metabolism regulates the generation of suppressive myeloid cells in the TME.

Here, we identified that hematopoietic precursor cells were enriched in several human cancers. These hematopoietic precursor cells can further differentiate into immature myeloid cells (IMC) with strong immunosuppressive capacity. To explore how metabolism regulates the generation of IMCs in the TME, we used an *in vitro* model to induce IMCs from $CD34^+$ precursors with

[1]Sun Yat-sen University Cancer Center, State Key Laboratory of Oncology in South China, Collaborative Innovation Center for Cancer Medicine, Guangzhou, P.R. China. [2]MOE Key Laboratory of Gene Function and Regulation, State Key Laboratory of Biocontrol, School of Life Sciences, Sun Yat-sen University, Guangzhou, P.R. China. [3]First Affiliated Hospital, Sun Yat-sen University, Guangzhou, P.R. China.

Note: Supplementary data for this article are available at Cancer Immunology Research Online (http://cancerimmunolres.aacrjournals.org/).

W.-C. Wu and H.-W. Sun contributed equally to this article.

Corresponding Author: Limin Zheng, Sun Yat-sen University, 651 Dongfeng Road East, Guangzhou 510060, P.R. China. Phone: 86-20-84112163; Fax: 86-20-84112169; E-mail: zhenglm@mail.sysu.edu.cn

Cancer Immunol Res 2019;7:1605–18

doi: 10.1158/2326-6066.CIR-18-0902

GM-CSF and G-CSF. Our work revealed that generation of IMCs relied on glutaminolysis, regardless of glucose availability. Glutamine-derived α-ketoglutarate (αKG) supported the expansion of IMCs, and glutamate, another intermediate, conferred the suppressive capacity through the NMDA receptor axis. Moreover, inhibition of glutaminase GLS1 improved the therapeutic efficacy of anti–PD-L1 treatment in an ICB-resistant mouse model. Thus, the glutamine metabolism of suppressive myeloid cells is a promising target to relieve the resistance of ICB therapy.

Materials and Methods

Materials

The detail of materials used in this article is summarized in Supplementary Table S1.

Human subjects

Peripheral blood, cord blood, non-tumor, and tumor tissue samples were obtained from the Cancer Center or the First Affiliated Hospital of Sun Yat-Sen University. All patients with cancer were pathologically confirmed without previous anticancer therapy, and individuals with concurrent autoimmune disease, HIV, or syphilis were excluded. Before processing, samples were shortly stored at 4°C refrigerator. All samples were coded anonymously in accordance with local ethical guidelines (as stipulated by the Declaration of Helsinki), and written informed consent was obtained. The protocol was approved by the Review Board of Sun Yat-Sen University.

Paired fresh tumor and non-tumor tissues from patients with hepatocellular ($n = 20$), breast ($n = 17$), and colorectal ($n = 40$) carcinomas were used for the isolation of tissue-infiltrating leukocytes, and for IHC and immunofluorescence staining. Peripheral blood samples from 27 patients with hepatocellular ($n = 11$), breast ($n = 5$), and colorectal ($n = 11$) carcinomas were taken before treatment. Control blood samples were obtained from 15 healthy donors, all negative for HCV, HBV, HIV, and syphilis, who had routine physical examinations at our cancer center.

Isolation of mononuclear cells

Peripheral leukocytes were isolated by Ficoll density gradient centrifugation. Infiltrated leukocytes from fresh tumor and non-tumor tissues were obtained as described in our previous studies (24). Liver, breast, and colon tissue biopsy specimens were cut into small pieces and digested in RPMI-1640 supplemented with 0.05% collagenase type IV (Sigma-Aldrich), 0.002% DNase I (Roche), and 20% fetal calf serum (FCS, HyClone Laboratories). The dissociated cells were then filtered through a 150-μm mesh and the mononuclear cells (MNC) were obtained by Ficoll density gradient centrifugation. The MNCs were washed and resuspended in media supplemented with 1% heat-inactivated FCS for FACS analysis.

Fresh tumor tissues from patients with breast ($n = 8$) and colorectal ($n = 11$) carcinomas were used for the detection of tissue-infiltrating $CD133^+$ cells by flow cytometry, and the clinical information of these patients was summarized in Supplementary Table S2.

In vitro methylcellulose colony-forming cell assay

$CD133^+$ cells were purified from tumor-infiltrating MNCs in colon and breast cancer patients with CD133 Isolation Kit (Miltenyi Biotec, cat. #130-097-049). The isolated cells were plated and cultured in Methocult H4034 Optimum media (STEMCELL Technologies, cat. #04034). Colonies were assigned scores after 14 to 16 days of culture on the basis of morphology according to the Atlas of Human Hematopoietic Colonies (STEMCELL Technologies, cat. #28700). The types and frequency of colonies were then recognized and counted manually under inverted microscope.

Suppressive IMC differentiation from tumor-infiltrating HPCs

$CD133^+$ HPCs were isolated from tumor tissues of colon and breast cancer patients. After that, cells were seeded at $1–2 \times 10^5$/well in 24-well plates and cultured in complete medium containing 10% heat-inactivated fetal bovine serum (FBS) supplemented with GM-CSF (40 ng/mL, R&D Systems, cat. #215-GM-010) and G-CSF (40 ng/mL, R&D Systems, cat. #214-CS-025) for 3 days. Differentiated cells were further cocultured 1:1 with allogenic T cells at 37°C in a 5% CO_2-humidified atmosphere for another 6 days.

Expansion of human $CD34^+$ progenitor cells

The $CD34^+$ cells were expanded as described in our previous work (25). In brief, $CD34^+$ cells were purified from fresh human cord blood or peripheral blood of healthy donors using a direct CD34 progenitor cell isolation kit, according to the manufacturer's instructions (Miltenyi Biotec, cat. #130-046-702). These $CD34^+$ cells were plated at 5×10^4 cells/mL in 6-well plates (Corning) with 3 mL/well of HSC expansion media (StemSpan SFEM, Stem Cell Technologies) supplemented with 100 ng/mL SCF, 100 ng/mL FLT-3L, 100 ng/mL TPO, and 20 ng/mL IL3 (R&D). The cells were cultured at 37°C in 5% CO_2 for 7 days. Fresh expansion media were changed on days 3 and 5. The cell density was kept at about $3–5 \times 10^5$ cells/mL. The information of media and cytokines was summarized in Supplementary Table S1.

Generation of $CD34^+$ cell–derived suppressive IMCs

The suppressive IMCs were induced by GM-CSF (40 ng/mL) and G-CSF (40 ng/mL) as described in our previous work (25). To obtain $CD34^+$ precursor–derived IMCs, the expanded $CD34^+$ cells were plated at 2.5×10^5/well in 24-well plates in complete DMEM supplemented with GM-CSF (40 ng/mL) and G-CSF (40 ng/mL), and cultured at 37°C in 5% CO_2-humidified atmosphere for 3 to 4 days. The information of cytokines was summarized in Supplementary Table S1.

In vitro differentiation assays

For experiments performed in the absence of glucose or glutamine, cells were differentiated in DMEM without glucose or glutamine (GIBCO) supplemented with BSA (1.5 g/L, GIBCO), GM-CSF (40 ng/mL), and G-CSF (40 ng/mL). Glucose utilization was blocked by addition of 2-DG (1 mmol/L, Sigma-Aldrich). Glutamine utilization was blocked, as indicated, by addition of BPTES (20 μmol/L; APExBIO), DON (50 μmol/L; Sigma-Aldrich), or aminooxyacetic acid (AOA) (1 mmol/L, Sigma-Aldrich), and rescue experiments were performed in the presence of DMK (7 mmol/L, Sigma-Aldrich), Embryomax nucleosides mix (Merck-Millipore), or desaturated lysophospholipid (C18:1; 20 μmol/L, Avanti polar lipids). These drugs were dissolved in DMSO or phosphate-buffered saline (PBS) as appropriate. The chemicals used in cell culture were summarized in Supplementary Table S1.

siRNA transfection

$CD34^+$ cells were cultured in expansion media for 5 days. Thereafter, they were left untreated or transfected with 40 nmol/L of a negative control siRNA or an ASCT2-specific siRNA (si-ASCT2#1: 5′-CCT GGG CTT GGT AGT GTT T-3′ or si-ASCT2#2: 5′-CCT GGA TCT TGC GAG AAA T-3′) using Lipofectamine-RNAi MAX (Invitrogen). After transfection for 48 hours, cells were collected, washed, and cultured in complete DMEM supplemented with GM-CSF and G-CSF for 3 days.

Coculture of IMCs with pan T cells

IMCs were resuspended in PBS and centrifuged twice to discard chemical in the culture media. Washed IMCs were cocultured with carboxyfluorescein diacetate succinimidyl ester (CFSE)-labeled T cells in the presence of coated anti-CD3 and soluble anti-CD28 antibody.

Pan T cells were purified from peripheral blood of healthy donors using a Pan T-cell Isolation Kit (Miltenyi Biotec, cat. #130-096-535). Pan T cells and splenocytes were stained with 2.5 μmol/L CFSE for 15 minutes before stimulation, according to the manufacturer's instructions (Invitrogen Molecular Probe, cat. #C34554). After CFSE staining, pan T cells or splenocytes were cultured only or were cocultured with washed IMCs (at a 1:1 ratio) in the presence of 2.5 μg/mL coated anti-CD3 (human: eBioscience, cat. #16-0037-85; mouse: BioLegend, cat. #100314) and 5 μg/mL soluble anti-CD28 (human: eBioscience, cat. #16-0289-85; mouse: BioLegend, cat. #102112) at 37°C in a 5% CO_2-humidified atmosphere for 6 days. Subsequently, the cells were collected, stained with surface markers, and analyzed by flow cytometry.

Cell lines and cell culture

4T1 (ATCC, CRL-2539) cells were obtained in 2014. 4T1 cells were cultured with RPMI-1640 medium (Gibco) supplemented with 10% FBS, penicillin (100 U/mL), streptomycin (100 mg/mL) at 37°C in 5% CO_2-humidified atmosphere, and were used for experiments within 10 passages. The cell line was tested to ensure negativity for *Mycoplasma*. This cell line was not reauthenticated within the past year.

Mice

Female BALB/c mice (6–8 weeks of age) were purchased from Guangdong Medical Laboratory Animal Center (Guangzhou, China). All mice were maintained under specific pathogen-free conditions in the animal facilities of Sun Yat-sen University Cancer Center (Guangzhou, China), and all animal experiments were performed according to state guidelines and approved by the IACUC of Sun Yat-sen University.

Tumor challenge and treatment experiments

In the 4T1 tumor model, 2×10^5 cells were injected subcutaneously into the flank of BALB/c mice, and tumor growth was monitored for up to 25 days. Tumor dimensions were measured with caliper once when tumors were palpable. Tumor volumes were calculated using the equation $(l^2 \times w)/2$. Mice cage and treatment allowance were randomized 7 days after tumor implantation. For therapeutic treatment, anti–PD-L1 antibody (200 μg per mouse, clone 10F.9G2, Bio X Cell, cat. # BE0101) or the corresponding IgG2b isotype control (Bio X Cell, cat. # BE0090) in 100 μL PBS was administered intraperitoneally to mice, twice a week for 2 weeks. For glutamine metabolism studies, mice were treated with the selective glutaminase inhibitor BPTES (12.5 mg/kg, ApexBio, cat. # B6008) or vehicle intraperitoneally twice a week.

Flow cytometry

The flow cytometry was performed as previously described (25). For surface marker staining, MNCs from peripheral blood, fresh tissue biopsy specimens or *in vitro* cultured cells were prepared and suspended in PBS supplemented with 1% heat-inactivated FCS. In some experiments, the cells were stained with surface markers, fixed and permeabilized with the Intracellular (IC) Fixation Buffer (00-8222, eBioscience) or Foxp3/Transcription Factor Fixation/Permeabilization Concentrate and Diluent (00-5521, eBioscience) reagent, and finally stained with related Abs. Data were acquired on a Gallios flow cytometer (Beckman Coulter) and analyzed with Kaluza 1.2 software (Beckman Coulter).

For cell sorting, cells from *in vitro* culture systems were resuspended in sorting buffer (1 × PBS; 3% FBS [v/v]; 3 mmol/L EDTA [v/v]) before sorting with a MoFlo XDP instrument (Beckman Coulter). DAPI was used for exclusion of dead cells (eBioscience). The fluorochrome-conjugated Abs used were summarized in Supplementary Table S1.

IHC and immunofluorescence

Paraffin-embedded cancer samples were cut into 4-μm sections and processed for IHC or immunofluorescence staining, as previously described (24). In brief, the sections were sequentially deparaffinized and rehydrated with xylene and a decreasing ethanol series. Then, the slides were soaked in 0.3% H_2O_2 for 10 minutes to quench endogenous peroxidase activity and boiled in 10 mmol/L citrate buffer (pH 6.0) for 10 minutes for heat-induced epitope retrieval. The tissues were stained with rabbit anti-human CD11b (dilution 1:500, Invitrogen, cat. # PA5-29633) and rabbit anti-human Glut1 (dilution 1:500, Millipore, cat. # 07-1401) or rabbit anti-human ASCT2 (dilution 1:500, Novus, cat. # NBP1-89327), or rabbit anti-human xCT (dilution 1:500, Novus, cat. # NB300-318). Signal in chromogenically labeled slides was visualized with DAB by horseradish peroxidase–conjugated anti-rabbit/mouse Dako REAL EnVision detection systems (Dako, cat. # K5007) and counterstained with Mayer's hematoxylin. Signal in immunofluorescently labeled slides was visualized with AlexaFluor 488, AlexaFluor 594, and AlexaFluor Cy5 TSA Kits (Invitrogen), and nuclei were visualized with Prolong Gold Antifade Reagent with 4′,6-diamidino-2-phenylindole (DAPI; Invitrogen). The images were viewed by optical microscope or scanning confocal microscope (Leica) and analyzed with LAS AF Lite software. All stained slides were evaluated in a blinded fashion by 2 pathologists. The antibodies were summarized in Supplementary Table S1.

XF extracellular flux analyzer experiments

Single-cell suspensions from *in vitro*–induced IMCs were plated in XF24 Cell Culture Microplates (Seahorse Bioscience) previously coated with Cell-Tak (BD Biosciences, cat. # 354240) at a cellular density of 1×10^4 cells/well. For oxygen consumption rates (OCR) determination, cells were incubated in XF Base Medium (Seahorse Bioscience) supplemented with 2 mmol/L glutamine, 10 mmol/L glucose, and 1 mmol/L pyruvate for 1 hour, prior to the measurements using the XF Cell Mito Stress Kit (Seahorse Bioscience). Concentrations of oligomycin and

FCCP were both 1 μmol/L. For glycolytic metabolism measurements, cells were incubated in XF Base Medium supplemented with 2 mmol/L glutamine prior to injections using the Glycolytic Test kit (Seahorse Bioscience). Experiments were run in an XFe24 analyzer (Seahorse Bioscience). Lactate production was measured by colorimetric assay (BioVision). The information of these assay kit was summarized in Supplementary Table S1.

RNA preparation and real-time PCR

Total RNA was isolated using TRIzol reagent (Life Technologies, cat. #15596-018). Aliquots containing 2 μg of total RNA were reverse transcribed using MMLV reverse transcriptase (Promega, cat. #M1701). PCR was performed in triplicate using SYBR Green Real-time PCR MasterMix (TOYOBO, cat. #QPS-201) in a Roche LightCycler 480 System. Expression levels were determined using threshold cycle (Ct) values normalized to *ACTB* (ΔCt) and expressed with $2^{-\Delta Ct}$. All results are presented in arbitrary units relative to human *ACTB* mRNA expression. The specific primers used in RT-PCR were summarized in Supplementary Table S1.

Immunoblotting

The proteins from IMCs were extracted with RIPA buffer (Thermo Fisher Scientific, cat. #89900). The protein concentrations of cell lysates were determined by BCA protein assay kit (Thermo Scientific, cat. #23225). Equal amounts of cellular proteins were separated by 8% or 10% SDS-PAGE, immunoblotted with anti-Arginase1 Ab and anti-β-actin, and visualized by ChemiDoc Imaging Systems (Bio-Rad) with ECL kit (Millipore, cat. #WBKLS0500). The antibodies used in immunoblotting were summarized in Supplementary Table S1.

Microarray data accession numbers

All microarray data are publicly available in the GEO database under accession number GEO GSE92367.

Statistical analysis

All experiments were performed using at least 3 different samples. Two-tailed Student *t* test and one-way ANOVA with Bonferroni adjustment were performed, and $P < 0.05$ was considered statistically significant. All analyses were performed using SPSS 19.0 (SPSS).

Results

Human tumor-infiltrating HPCs can form suppressive IMCs

We previously found that circulating and splenic HPCs are myeloid biased in cancer and could be recruited to tumor sites (11, 25). To investigate the differentiation potential of tumor-infiltrating HPCs, $CD133^+$ cells were isolated from tissues of colon and breast cancer patients. Their differentiation capacity was tested by the methylcellulose assay. Apart from erythroid differentiation potential, HPCs enriched in tumor tissues were also capable of forming granulocyte-macrophage colonies (CFU-GM; Fig. 1A), similar to those from peripheral blood (25). The HPCs from tumor tissues can differentiate into IMCs in response to tumor-secreting cytokines, such as GM-CSF and G-CSF (26, 27). When cocultured with T cells activated by anti-CD3 and anti-CD28 antibodies, these IMCs exhibited strong suppressive activity against both Th and Tc cells (Fig. 1B).

To dissect the composition of suppressive myeloid cells, we used flow cytometry to characterize different subsets of myeloid cells ($CD45^+CD33^+HLA\text{-}DR^{low/-}CD3^-CD19^-CD56^-7AAD^-$; ref. 28) in paired tumor and adjacent non-tumor tissues from colon, breast, and liver cancer patients. In addition to classic myeloid derived suppressor cells (MDSC), a $CD33^+CD11b^{low/-}$ myeloid subset was enriched by tumor tissues (21.3% ± 3%) compared with non-tumor tissues (5.2% ± 0.9%; Fig. 1C and D, and Supplementary Fig. S1). Most of these $CD33^+CD11b^{low/-}$ cells had low expression of mature myeloid markers, including CD14 and CD15 (Fig. 1C; Supplementary Fig. S1), but maintained the expression of the stem/progenitor cell marker CD133 (Supplementary Fig. S2A). Thus, these cells could be characterized as immature myeloid cells or early-stage MDSCs (28). Compared with monocytic MDSC (M-MDSC) and polymorphonuclear MDSC (PMN-MDSC) subsets, these IMCs expressed more of the proliferation marker Ki67 (7.2% ± 1.0% IMC, 0.17% ± 0.06% M-MDSC, 0.17% ± 0.05% PMN-MDSC) and macrophage colony-stimulating factor receptor (M-CSFR; MFI: 25.9 ± 3.1 IMC, 7.6 ± 1.1 M-MDSC, 7.9 ± 1.1 PMN-MDSC), a key marker of suppressive myeloid cells (refs. 29, 30; Fig. 1E–H; Supplementary Fig. S2B). These results indicate that tumor-infiltrating HPCs are sources of IMCs in human cancers.

Human suppressive IMCs differentiated from HPCs exhibited high glycolytic metabolism

The TME is known to induce metabolic changes in immune cells, regulating their phenotype and function. To examine the metabolic status of IMC subsets, we assessed the expression of glucose transporter Glut1 (SLC2A1). The results showed that Glut1 was only expressed in a minor proportion of M-MDSC and PMN-MDSC subsets from tumor (2.9% ± 0.5%) or non-tumor (0.7% ± 0.1%) tissues (Fig. 1C and I; and Supplementary Fig. S1), and was rarely detectable on circulating mature myeloid cells (Supplementary Fig. S2C). In contrast, the expression of Glut1 was selectively upregulated on IMCs derived from tumor tissues (37.2% ± 3.5% tumor vs. 10.8% ± 1.4% non-tumor; Fig. 1C and I; Supplementary Fig. S1). By using confocal microscopic analysis, we further confirmed the Glut1 expression on myeloid cells that were localized in the invasive tumor margin *in situ* (Supplementary Fig. S2D). The selective upregulation of Glut1 on the IMCs indicates that a glycolytic mode of energy metabolism might be critical for the generation of IMCs.

We and others have shown that G-CSF and GM-CSF are the dominant cytokines that regulate myelopoiesis of HSPCs and induce subsequent accumulation of suppressive myeloid cells in several cancers (25, 31). There are limited available models that might reveal the differentiation process of human IMCs. To elucidate the potential metabolic mechanism that regulates the phenotype and function of IMC subsets, we used human hematopoietic progenitors and established a short-term culture system to reliably induce suppressive IMCs *in vitro* (25). During *in vitro* differentiation of IMCs, the expression of Glut1 was significantly upregulated (Fig. 2A), mainly on $CD11b^{low/-}$ cells (Supplementary Fig. S3A). A profound elevation of M-CSFR was observed on these IMC (Supplementary Fig. S3B). Importantly, the inhibition of M-CSFR by pretreatment with neutralizing antibody significantly attenuated the acquisition of suppressive function after the differentiation process, indicating that M-CSFR was a key component of IMC activation program *in vitro* (Supplementary Fig. S3C and S3D).

Next, we examined the bioenergetic profiling of HPC-derived IMCs using the Seahorse XF-analyzer platform. IMCs displayed an

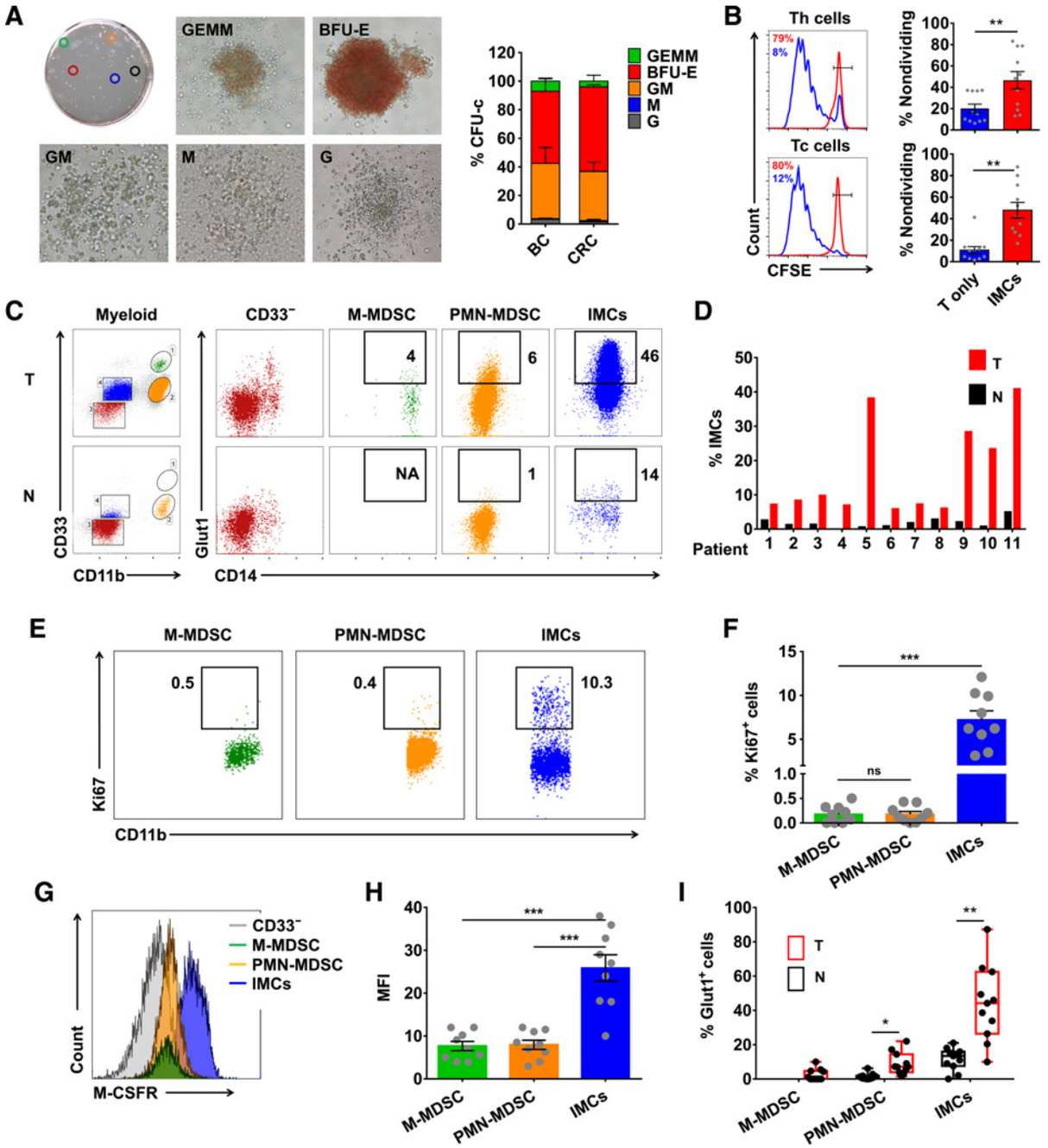

Figure 1.

Suppressive IMCs can be induced from tumor-infiltrating HPCs. **A,** Granulocyte–macrophage colony-forming units from tumor-infiltrating CD133$^+$ cells in colony-forming units in culture (CFU-c) assay. BFU-E, burst-forming unit-erythroid; G, granulocyte; GEMM, granulocyte, erythrocyte, macrophage, megakaryocyte; GM, granulocyte, macrophage; M, macrophage. CD133$^+$ cells isolated from colon ($n = 4$) and breast ($n = 4$) tumor tissues were tested in the CFU-c assay. Data, mean ± SEM. **B,** CD133$^+$ cells, isolated from colon and breast tumor tissues, were induced *ex vivo* by culture with combined GM-CSF and G-CSF for 3 days. After that, the differentiated cells were cocultured at 1:1 ratio with allogenic T cells. Data are from 11 patients and shown as mean ± SEM in **B**. *, $P < 0.05$; **, $P < 0.01$. **C,** Myeloid cells were isolated from paired colon tumor and non-tumor tissues, and gated in CD45$^+$HLA-DR$^{low/-}$CD3$^-$CD19$^-$CD56$^-$7AAD$^-$ cells. Representative FACS analysis of cell-surface Glut1 expression in different myeloid subsets gated by CD33 and CD11b. **D,** Summary of the frequency of IMCs in total suppressive myeloid cells. Representative FACS analysis (**E**) and comparison (**F**) of Ki67 expression between M-MDSC, PMN-MDSC, and IMC subsets. **G** and **H,** Representative FACS analysis of M-CSFR expression in different myeloid subsets from colon cancer (**G**). The mean fluorescence intensity (MFI) of M-CSFR expression was determined by FACS, and its expression in each subset of suppressive myeloid cells is summarized (**H**). Data are from 9 colon cancer patients and shown as mean ± SEM in **E–H**. ***, $P < 0.001$. **I,** Glut1 expression in each subset of myeloid cells from colon cancer samples. Data are from 11 patients and shown as mean ± SEM. *, $P < 0.05$; **, $P < 0.01$. The statistical significance of differences between groups was determined using a paired Student *t* test.

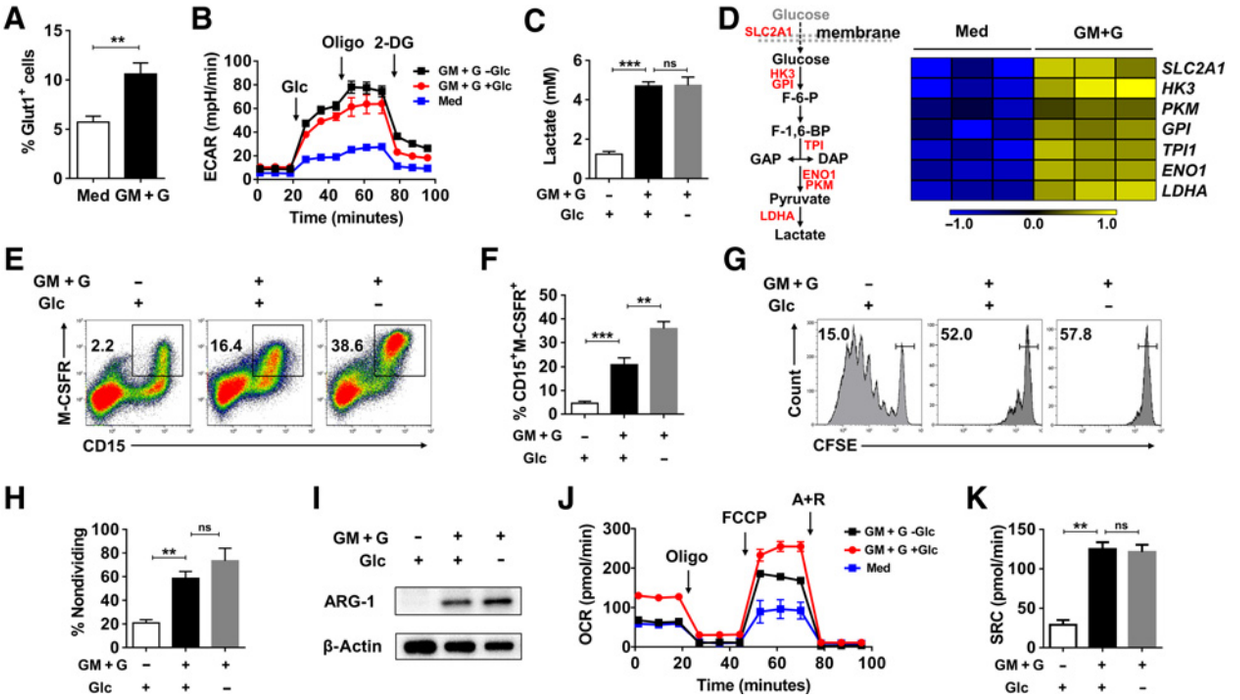

Figure 2.

The generation of functional IMCs is accompanied by increased glycolysis but not affected by glucose deprivation. **A,** Surface Glut1 expression of cells induced with combined cytokines (GM-CSF + G-CSF) or medium alone (Med) was measured. Data are from six independent experiments and are shown as mean ± SEM. **, $P < 0.01$. **B,** Extracellular acidification rate (ECAR) of untreated cells or IMCs induced under normal or glucose-deprived conditions was assessed after the addition of glucose (gluc), oligomycin (oligo), and 2-deoxyglucose (2-DG) at the indicated times. **C,** Total lactate produced by cells induced at indicated conditions was measured. Data are from three independent experiments and are shown as mean ± SEM. ***, $P < 0.001$. ns, not significant. **D,** Diagram of the glycolytic pathway, with molecules measured highlighted in red (left). RNA was isolated from untreated cells or IMCs and then used for real-time PCR analyses of glycolytic molecules (right). Data are normalized and log transformed to show three independent experiments. **E** and **F,** Precursors were induced by combined GM-CSF and G-CSF in complete medium or glucose-deprived medium for 3 days. Representative FACS analyses of M-CSFR expression (**E**) and the summary of $CD15^+$M-$CSFR^+$ cell frequency (**F**). **G** and **H,** The proliferation of T cells cocultured with washed IMCs induced in medium with or without glucose was analyzed by FACS (**G**) and summarized (**H**). Data from six independent experiments shown as mean ± SEM in **E–H**. ***, $P < 0.001$. ns, not significant. **I,** Immunoblot for ARG1 in normal and glucose-deprived IMCs. **J**, Metabolic profile of normal and glucose-deprived IMCs. OCR were assayed by Seahorse XF24 Analyzer at different time points. Representative data from 1 of 4 donors; each condition was repeated 4 times. **K,** SRC of normal and glucose-deprived IMCs was determined. Data are from three independent experiments shown as mean ± SEM in **K**. **, $P < 0.01$. ns, not significant. The statistical significance of differences between groups was determined by a two-tailed Student *t* test.

approximately 3-fold increase in both the extracellular acidification rate (ECAR) and lactate production (Fig. 2B and C) compared with untreated cells. Accordingly, real-time PCR analysis revealed that these cytokine-induced IMCs upregulated expression of multiple proteins and enzymes involved in glycolysis. These include the transporter Glut1 (*SLC2A1*), glycolytic enzymes hexokinase 3 (*HK3*), glucose-6-phosphate isomerase (*GPI*), triosephosphate isomerase 1 (*TPI1*), enolase 1 (*ENO1*), pyruvate kinase muscle (*PKM*), and lactate dehydrogenase α (*LDHA*; Fig. 2D). These results indicated that human IMCs differentiated from HPCs exhibited high glycolytic metabolism.

IMCs can function normally and maintain catabolism in glucose-deprived conditions

We examined whether glucose affected IMCs function by inducing IMCs in normal or glucose-deprived medium. To our surprise, induction of IMCs in glucose-insufficient conditions did not impair the expression of suppressive molecule arginase 1 (ARG1) and the suppressive activity of IMCs, but slightly elevated the proportion of the $CD15^+$M-$CSFR^+$ subset in IMCs (Fig. 2E–I). Consistent with this finding, IMCs induced in glucose-deprived medium maintained high levels of catabolism (as indicated by lactate production and ECAR) with increased expression of Glut1 (Fig. 2B and C; Supplementary Fig. S4A). Although these cells reduced their basal and maximal OCR, their spare respiratory capacity (SRC) was unchanged in glucose-deprived conditions (Fig. 2J and K). Thus, our data indicated that IMCs could maintain normal catabolism to support their functional features under glucose-deprived conditions.

We also used 2-DG, a prototypical inhibitor of glycolysis via blocking hexokinase, to test the importance of glycolysis in IMC differentiation. Distinct from glucose deprivation, 2-DG treatment abolished the glucose uptake and lactate production of IMCs (Supplementary Fig. S4A–S4C). Moreover, 2-DG treatment inhibited the proliferation of $CD11b^{low/-}$ IMCs (Supplementary Fig. S4D and S4E) and markedly reduced the expression of M-CSFR and ARG1 of IMCs under both normal and glucose-deprived conditions (Supplementary Fig. S3B; Supplementary Fig. S4A, S4B, and S4F). CFSE assays showed that 2-DG treatment

also significantly attenuated the suppressive activity of IMCs on T cells (Supplementary Fig. S4G and S4H).

Given that hematopoietic precursors from peripheral blood could be directly recruited to tumor sites to differentiate into IMCs, we also used circulating $CD34^+$ cells from peripheral blood and obtained similar results (Supplementary Fig. S5). Thus, these data suggest that an alternative energy resource might be necessary to support the generation and suppressive activity of IMCs in glucose-insufficient conditions.

Glutaminolysis is the anaplerotic metabolic pathway for supporting IMC differentiation

We next performed microarray analysis to compare the transcriptional profiling from IMCs induced in normal and glucose-deprived conditions. Using the significance analysis of the microarray algorithm, we identified 575 glucose deprivation-induced genes, and 47 of them were metabolism-related genes. Using Gene Ontology enrichment analysis, we found that these 47 genes were enriched for the cellular amino acid metabolic process (Fig. 3A). Interestingly, glucose deprivation upregulated a set of genes in IMCs that have been implicated in glutaminolysis, including *GLS*, *GLUL*, *BCAT1*, *SLC1A3*, and *SLC7A11*, which was further confirmed by quantitative RT-PCR (Fig. 3B and C). In addition, *ASS1*, a key enzyme in the urea cycle that is metabolically linked with amino acid metabolism, was also upregulated in IMCs induced under glucose-deprived condition (Fig. 3B–E). These data strongly indicate that glutaminolysis might be an alternative metabolic pathway to support IMC generation in glucose-deprived conditions. To test this, cytokine-treated precursors were cultured with complete medium (CM), glucose-deprived medium (Non-glc), glutamine-deprived medium (Non-gln), or glucose and glutamine double-deprived medium (Non-glc-gln). Glutamine deprivation markedly reduced the proportion of the $CD15^+$M-$CSFR^+$ subset and the expansion capacity and suppressive activity of IMCs both in the presence and absence of glucose. The expression of Glut1 and ARG1 on IMCs was also markedly downregulated in IMCs after glutamine deprivation (Fig. 3F–I). Altogether, these data point to a crucial role of glutamine metabolism in the differentiation of IMCs in both normal and glucose-deprived conditions.

Blocking glutamine utilization abrogates the generation of functional IMCs

The uptake of glutamine is primarily mediated by the amino acid transporter ASCT2 (SLC1A5; ref. 32). To investigate the role of glutamine metabolism in the differentiation of IMCs, we first examined ASCT2 protein expression on induced IMCs and tumors *in situ*. ASCT2 is highly expressed on cytokine-induced IMCs and myeloid cells at the invasion margin of tumor tissues (Supplementary Fig. S6A and S6B). Next, we pursued an siRNA-mediated interference approach to determine whether ASCT2 was directly responsible for the observed glutamine-dependent effects on IMCs. The results showed that activation of IMCs, indicated by M-CSFR expression, was significantly attenuated by treatment with si*ASCT2* compared with cells treated with scrambled sequence (Supplementary Fig. S6C and S6D). In addition, 2-DG treatment and glucose deprivation had obviously different effects on IMCs metabolic reprogramming. IMCs can acquire normal levels of ASCT2 expression in glucose-deprived conditions, while completely lost ASCT2 expression with 2-DG treatment (Supplementary Fig. S6B).

ASCT2 also transports other neutral amino acids, including alanine, serine, and cysteine. To determine whether the role of ASCT2 in IMCs is due to its capacity to transport glutamine, we blocked glutaminolysis with several inhibitors that act through different mechanisms (Fig. 4A). Mitochondrial utilization of glutamine occurs via the deamination of glutamate, a reaction catalyzed typically by either glutamate dehydrogenase (GDH) or transaminases. We detected significant upregulation of the expression of transaminases *PSAT1* and *GPT2* (Fig. 4B), but not *GDH* in cytokine-induced IMCs. This result pointed to the importance of transaminases in IMC differentiation. Indeed AOA, a pan transaminase inhibitor (33), markedly reduced the generation of functional IMCs (Fig. 4C–E). We also tested bis-2-(5-phenylacetamido-1,3,4-thiadiazol-2-yl)ethyl sulfide (BPTES) and 6-diazo-5-oxo-L-norleucine (DON), 2 mitochondrial glutaminase inhibitors that target glutamine metabolism (34), and observed that treatment significantly abrogated IMCs commitment, as shown by the reduction of functional IMCs and ARG1 expression (Fig. 4C–E).

Glutamine-derived αKG is crucial for the expansion of IMCs by restoring the tricarboxylic acid cycle

Generally, glutamine is a nonessential amino acid that can be converted to αKG and utilized in the tricarboxylic acid (TCA) cycle by cells. Glutamine is also converted to glutamate by glutaminase (GLS) in nitrogen-donating reactions for nucleotide synthesis (12, 35). To elucidate the mechanisms by which glutamine supports the differentiation and function of IMCs, we carried out rescue experiments with supplementation of nucleotides and αKG, glutamine-derived metabolic products, in glutamine-deprived conditions. Supplementing cells with nucleosides did not rescue the commitment of glutamine-deprived IMCs. In contrast, supplementation with dimethyl-αKG (DMK), a cell-permeable form of αKG, could largely restore the Glut1 expression and cell proliferation capacity of IMCs (Fig. 5A and B). DMK only partially rescued the production of $CD15^+$M-$CSFR^+$ cells (Fig. 5A and B). Combination of nucleosides with DMK did not have synergistic effects (Fig. 5A and B).

αKG can be either oxidized to succinate (standard TCA cycle reaction) or reductively carboxylated to citrate, which can be further synthesized to lipids (36, 37). We next investigated which of these pathways glutamine-derived αKG contributed to. Lipids incorporated from glutamine can be rescued by the desaturated lysophospholipid (C18:1; ref. 38). However, we found that this could not rescue the glutamine-dependent commitment of IMCs (Supplementary Fig. S7A). We then analyzed OCR, an estimation of OxPhos, to determine whether αKG could rescue the TCA cycle of IMCs in glutamine-depleted conditions. The results showed that addition of DMK could effectively restore both the basal and maximal OCR of IMCs in glutamine-deprived condition (Fig. 5C). These data demonstrate a critical role of glutamine-derived αKG in supporting the proliferation and differentiation of IMCs via restoring the TCA cycle.

Glutamate can promote late-stage IMC activation through NMDAR

The generation of functional IMCs from hematopoietic precursors is thought to be a two-stage process, myeloid differentiation followed by activation (39). We next examined the kinetic effects of glutamine on myeloid differentiation and cellular

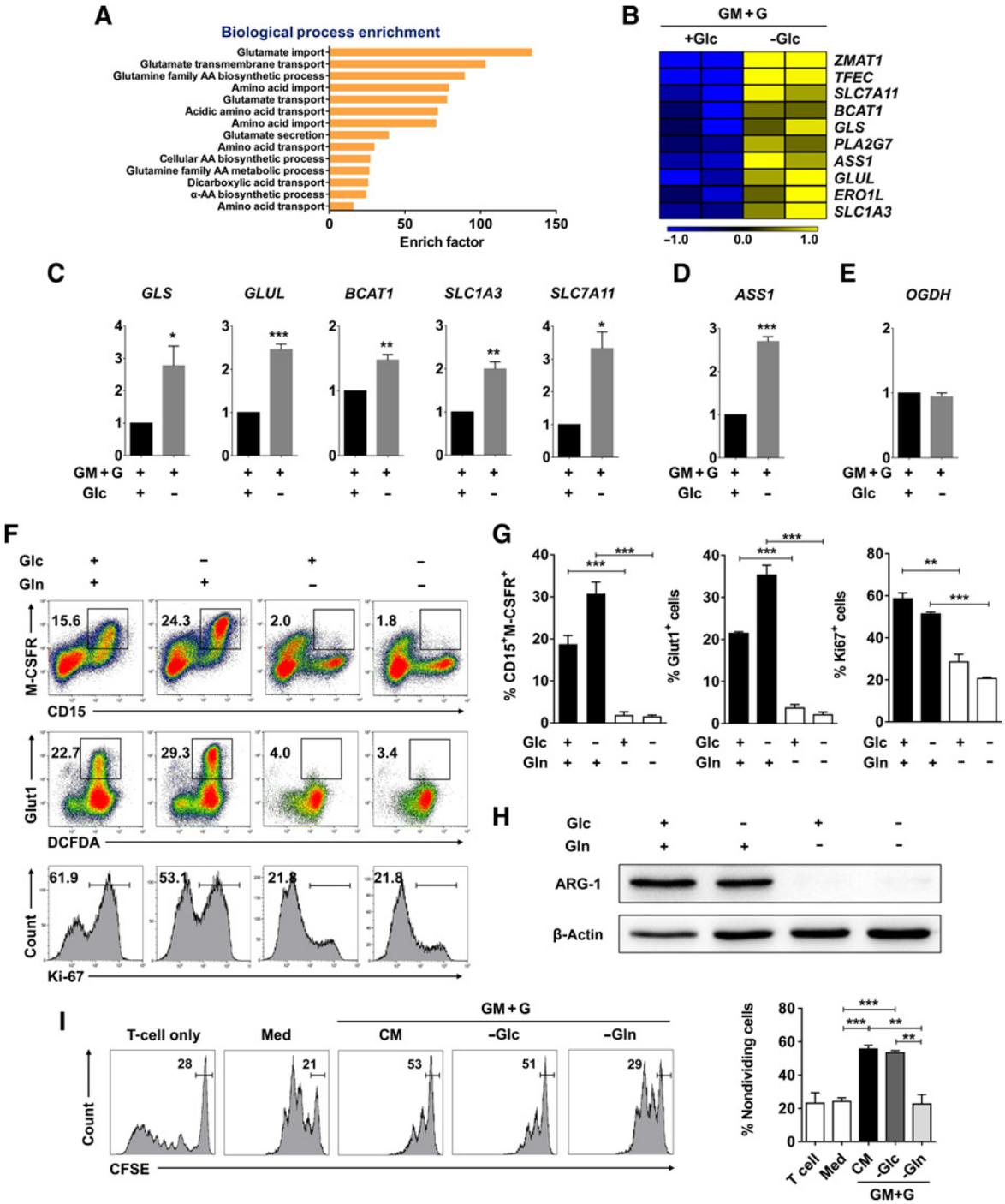

Figure 3.

Glutamine is required for the expansion and activation of IMCs under both normal and glucose-deprived conditions. **A,** Biological process analyses of transcriptomes of normal versus glucose-deprived IMCs identified cellular amino acid metabolic process as the most differentially regulated gene set. **B,** Heat map of differentially regulated genes in the cellular amino acid metabolic process gene set in normal and glucose-deprived IMCs induced by GM-CSF and G-CSF. Normalized and log-transformed data are shown. **C–E,** Validation of microarray data by quantitative RT-PCR. Data from three independent experiments shown as mean ± SEM in **C–E**. *, $P < 0.05$; **, $P < 0.01$; ***, $P < 0.001$. **F** and **G,** Representative FACS analyses of M-CSFR, cell-surface Glut1, and cell proliferation (**F**) of IMCs induced with indicated conditions. Statistical analysis of at least four independent experiments shown as mean ± SEM in **G**. **, $P < 0.01$; ***, $P < 0.001$. **H,** Immunoblot for ARG1 expression in IMCs induced with indicated conditions. **I,** FACS analyses of the immune-suppressive activity of IMCs induced by indicated conditions. CM, complete medium. Data represent four independent experiments and are shown as mean ± SEM in **I**. **, $P < 0.01$; ***, $P < 0.001$. A two-tailed Student *t* test was applied to determine the statistical significance.

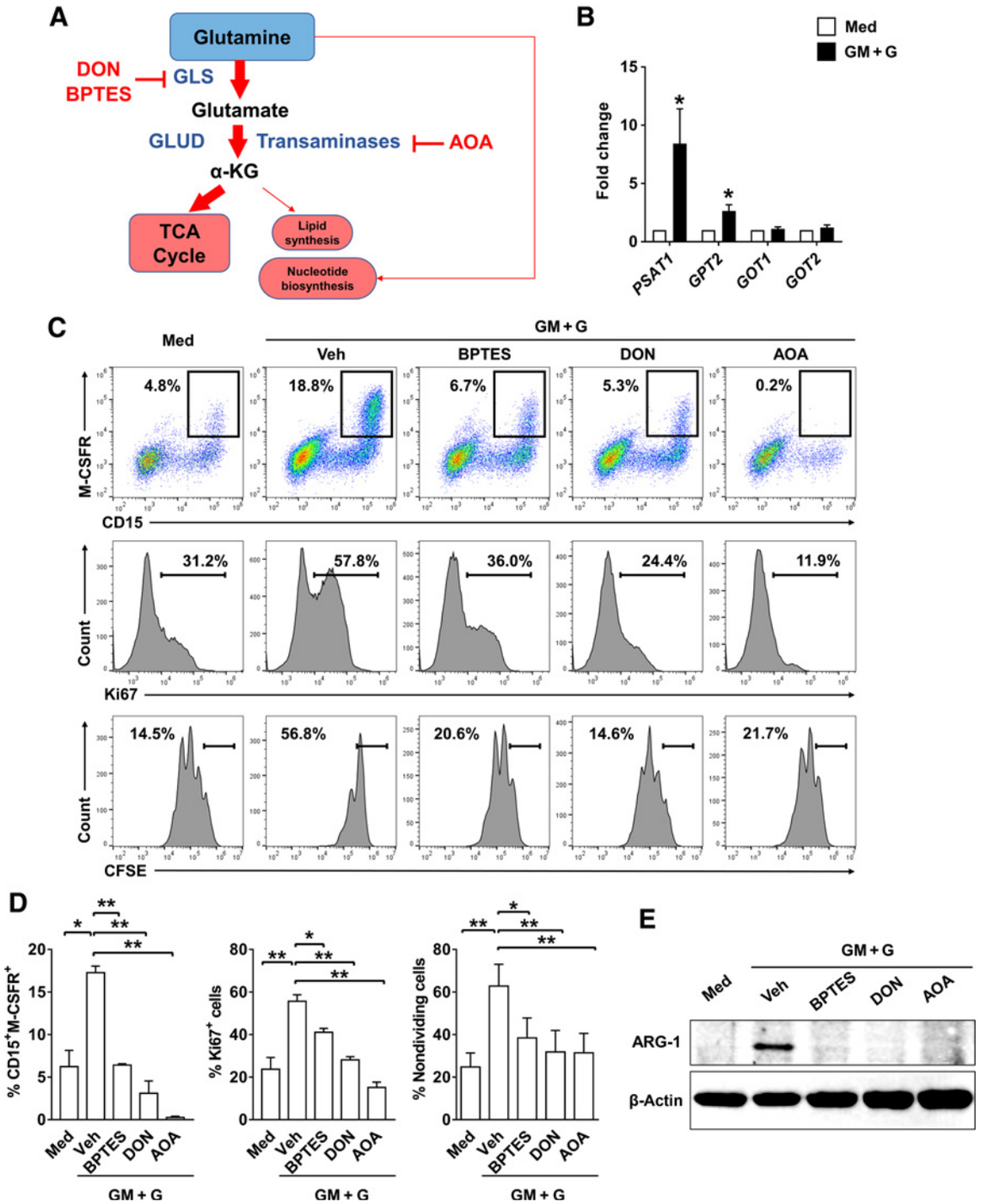

Figure 4.

Blocking glutamine metabolism abrogates the generation of functional IMCs. **A,** Schematic representation of glutamine conversion to α-ketoglutarate (αKG) with key enzymes indicated in blue and inhibitors, bis-2-(5-phenylacetamido-1,3,4-thiadiazol-2-yl) ethyl sulfide (BPTES), 6-diazo-5-oxo-L-norleucine (DON), and AOA, shown in red. **B,** Relative gene expression of transaminases in cytokine-induced IMCs. Data represent five independent experiments and are shown as mean ± SEM in **B**. *, $P < 0.05$. **C** and **D,** IMCs induced in the absence (Veh, vehicle) or presence of BPTES (20 μmol/L), DON (50 μmol/L), or AOA (1 mmol/L) for 3 days. The expression of M-CSFR markers, cell proliferation, and suppression capacity of IMCs was monitored at day 3 of differentiation (**C**). Statistical analysis of at least four independent experiments shown as mean ± SEM in **D**. **, $P < 0.01$; ***, $P < 0.001$. **E,** Immunoblot for ARG1 expression in IMCs induced with indicated conditions. A two-tailed Student *t* test was applied to compare the difference between indicated groups.

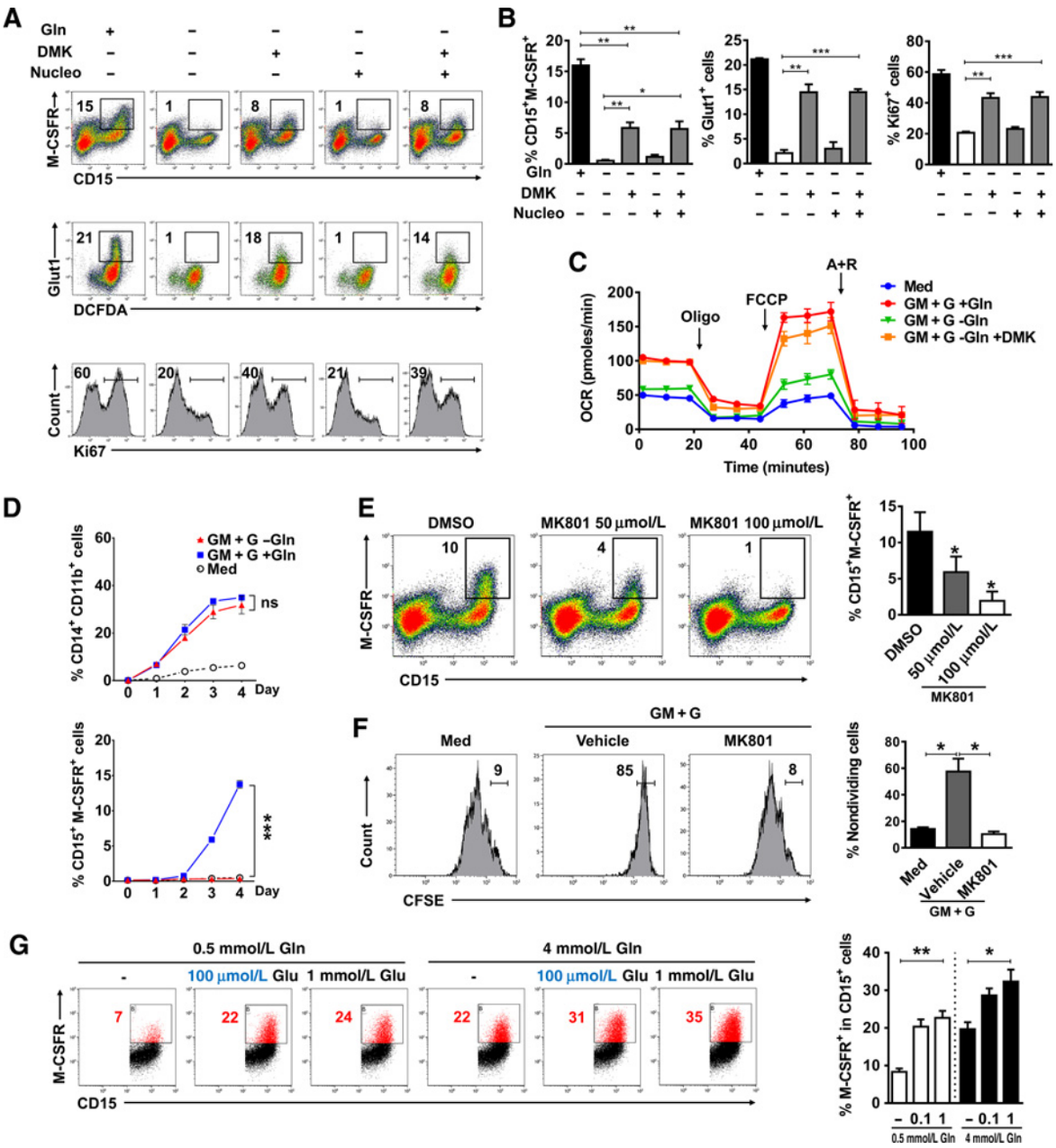

Figure 5.

Glutaminolysis supports the generation of IMCs with glutamine-derived α-ketoglutarate and the glutamate–NMDA receptor axis. **A,** The contribution of glutamine-derived α-KG and nucleotide biosynthesis in IMC differentiation was assessed by supplementing $CD34^+$ progenitors with DMK (7 mmol/L) or nucleosides cultured in the absence of glutamine. The expression of the activation marker M-CSFR, glycolytic marker Glut1, and cell proliferation was monitored at day 3 (representative data shown). **B,** The percentage of $CD15^+M\text{-}CSFR^+$ cells, the expression of cell-surface Glut1, and cell proliferation are summarized. Data are from three independent experiments shown as mean ± SEM in **B**. *, $P < 0.05$; **, $P < 0.01$; ***, $P < 0.001$. **C,** OCR determined by the Seahorse XF24 Analyzer with subsequent injections of oligomycin (Oligo), FCCP, and antimycin plus rotenone (A + R) into the culture medium at the indicated times. The values were used to assess rescuing of the TCA cycle in IMCs. **D,** Precursors were induced by combined cytokines in complete medium or glutamine-deprived medium for 4 days. Kinetic effects of glutamine deprivation on the differentiation of $CD34^+$ precursors were monitored. Myeloid differentiation was indicated by the expression of CD11b and CD14, and IMC activation was shown by M-CSFR expression. Data from three independent experiments shown as mean ± SEM in **D**. ***, $P < 0.001$. ns, not significant. **E** and **F,** IMCs were induced by combined cytokines with DMSO or NMDAR inhibitor MK-801 at the indicated concentrations. The expression of M-CSFR was estimated at day 3 (representative data were shown; **E**). Cells cultured with DMSO (IMCs) or MK-801 (MK-801 treated) were cocultured with allogenic $CFSE^+$ T cells for 6 days. The suppressive activity of IMCs was then assessed by FACS analysis (**F**). Data from four independent experiments shown as mean ± SEM in **E** and **F**. *, $P < 0.05$; **, $P < 0.01$. **G,** IMCs were induced in normal and low concentrations of glutamine with the addition of indicated doses of glutamate. M-CSFR expression was monitored at day 3 and is shown as a percentage of $M\text{-}CSFR^+$ in $CD15^+$ cells. Data from three independent experiments shown as mean ± SEM in **G**. *, $P < 0.05$; **, $P < 0.01$. The difference between indicated groups was determined by a two-tailed Student *t* test.

expression of M-CSFR. The results showed that depletion of glutamine in culture media did not affect myeloid differentiation, but almost completely blocked expression of M-CSFR, the key component for activation of IMC-suppressive function (Fig. 5D).

The above results collectively indicate a critical role of glutamine metabolism in the activation of IMCs, a process that is independent of glutamine-derived nucleotide and lipid biosynthesis. Moreover, α-KG can only partially rescue the expression of M-CSFR. These results indicate that other component(s) in the glutamine metabolic pathway might contribute to IMC activation. Glutamate was originally found as a major excitatory neurotransmitter in the CNS and can also act as a signaling molecule in other tissues (40). Recent studies have shown that glutamate could regulate the activation and proliferation of T cells through the glutamate receptor NMDAR (41). Therefore, we examined the effect of the NMDAR inhibitor MK-801 on IMC activation. The results showed that treatment with MK-801 significantly reduced the expression of M-CSFR and immune-suppressive function of IMCs (Fig. 5E and F). We subsequently examined the effect of exogenous glutamate on IMC activation. In glutamine-insufficient culture conditions, glutamate at a low dose (100 μmol/L) could effectively restore M-CSFR expression. Interestingly, exogenous glutamate could also increase M-CSFR expression on IMCs under normal culture conditions (Fig. 5G). These data indicate a critical role of exogenous glutamate in IMC activation.

Although cancer cells utilize a large amount of glutamine for tumor growth, they also secrete the metabolite glutamate out to the TME. Glutamate secretion by cancer cells could be mediated by xCT (SLC7A11) cysteine/glutamate antiporter (42). Indeed, expression of xCT antiporter was markedly elevated in tumor tissues, including tumor stroma cells (Supplementary Fig. S7B and S7C). We subsequently examined the *in situ* distribution of xCT in sections of colon cancer tissues by confocal microscopy. xCT expression is closely linked with IMCs, and they are well colocalized at invasion margin of tumor tissues (Supplementary Fig. S7D). These data indicate that glutamate, as a metabolite from the TME, can be an important strategy for tumors to promote the activation of IMCs.

Inhibiting the glutamine metabolism of IMCs improves ICB therapy

Suppressive myeloid cells contribute to the resistance of ICB therapy by suppressing T-cell function (8). To find out the role of glutamine utilization in the generation of suppressive myeloid cells *in vivo*, we tested the effect of BPTES, a selective inhibitor of glutaminase GLS1, on the function of tumor-infiltrating myeloid suppressors in an ICB-resistant 4T1 tumor model. The myeloid cells were purified and cocultured with CFSE-labeled splenocytes from untreated tumor-free mice for 3 days. The suppressive function of tumor-infiltrating myeloid suppressors was significantly attenuated in the BPTES-treated group (Fig. 6A). Although glutamine metabolism is critical for many cancer cells, treatment with BPTES alone only had slight/negligible effect on tumor growth (Fig. 6B). However, BPTES enhanced the therapeutic efficacy of anti–PD-L1 treatment and delayed tumor growth (Fig. 6B). We examined the infiltration of tumor-infiltrating myeloid suppressors, as well as T cells in the 4T1 model. Although BPTES or anti–PD-L1 alone had a slight/negligible effect on the total number of $Ly6G^+$ myeloid suppressor cells in tumor tissues, BPTES treatment significantly decreased the expression of ARG1 on the myeloid cells (Fig. 6C and D). These data collectively indicated that targeting glutamine metabolism could abrogate the differentiation and suppressive function of tumor-infiltrating myeloid cells. Neither BPTES nor anti–PD-L1 alone could efficiently rescue the cytotoxic potential of tumor-infiltrating-T cells. The combination of both BPTES and anti–PD-L1 treatment markedly increased the percentage of $CD8^+$, $IFN\gamma^+$, and granzyme B^+ T cells in tumors (Fig. 6E–H). These data indicate that targeting the generation of suppressive myeloid cells from tumor-infiltrating HPCs by BPTES relieves the resistance to ICB therapy.

Discussion

Tumor-associated myeloid cells contain mixed groups of myeloid cells that are expanded and activated in tumor tissues (2). Here, we found that hematopoietic precursor cells are enriched in several types of human cancers. Tumor-infiltrating hematopoietic precursor cells can further differentiate into IMCs with strong immunosuppressive capacity. These IMC expressed high levels of the glucose transporter Glut1 and M-CSFR, a key marker of suppressive myeloid cells. *In vitro*, we demonstrated that the cytokines-induced immunosuppressive IMCs exhibited highly glycolytic metabolism. The generation of IMCs was not affected by glucose deprivation due to anaplerotic glutaminolysis. Glutaminolysis was an important catabolic pathway for the generation of myeloid suppressors. Glutamine supported the expansion of myeloid suppressors with glutamine-derived α-ketoglutarate (αKG) and regulated the activation and function of myeloid suppressors through the glutamate–NMDA receptor axis. These findings revealed a novel mechanism for the generation of functional IMCs in the TME.

The ability to access sufficient and appropriate nutrients is a fundamental requirement for cell activation and proliferation, particularly in the nutrition-limiting TME (18, 43, 44). Indeed, we found increased expression of Glut1 on IMCs isolated from human tumor tissues, indicating a strong need for glycolysis during IMC generation. Accordingly, cytokine-induced IMCs express high levels of Glut1 with upregulation of glycolytic enzymes and elevated glycolytic flux. However, the lactate production and differentiation of IMCs is not affected by glucose deprivation, which suggests the existence of an alternative metabolic switch in glucose-limiting conditions. Our data indicate that tumor-associated glycolysis may affect the IMC compartment, and glutamine is one critical element for the differentiation and suppressive function of IMC in the TME. However, it remains unclear how tumor-associated metabolism regulates the myeloid compartment at the genetic, transcriptional, and/or translational levels. In contrast, the glycolysis inhibitor 2-DG could block the metabolic reprogramming during IMC differentiation, probably due to its inhibiting effect on anaplerotic glutaminolysis, which was indicated by a reduced ASCT2 expression.

Glutamine is a primary nitrogen source and is second only to glucose as a carbon source for energy production and anabolic processes (45). The present study revealed that glutamine metabolism is both necessary and sufficient to support the generation of functional IMCs under normal and glucose-insufficient conditions. However, this glutamine-dependent process is neither due to the nitrogen-donating reactions of nucleotide synthesis, nor due to the reductive carboxylation of fatty acid production. Rather, it is glutamine-derived αKG that generates substantial respiration capacity for IMC differentiation by restoring the TCA cycle. The essential role of glutamine in fueling mitochondrial

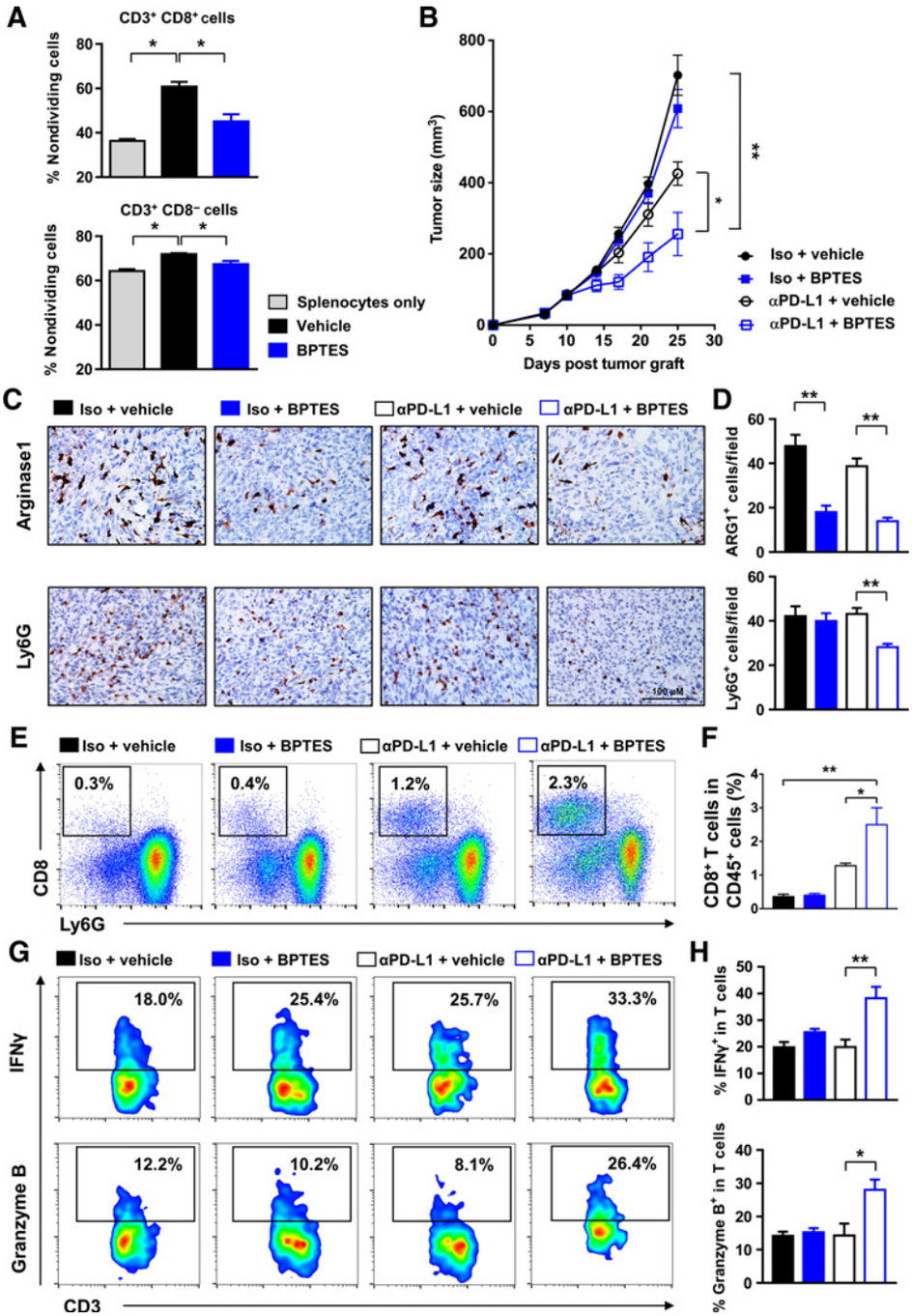

Figure 6.

Inhibiting the glutamine metabolism of suppressive myeloid cells could relieve the resistance to ICB therapy. **A,** Tumor-infiltrating myeloid suppressors from mice treated with vehicle or 12.5 mg/kg BPTES twice a week for 2 weeks were purified and cocultured with CFSE-labeled splenocytes for 3 days in the presence of 2.5 μg/mL coated anti-CD3 and 5 μg/mL soluble anti-CD28 antibody. The proliferation of splenocytes was monitored by flow cytometry and summarized ($n = 3$/group). Data from two independent experiments shown as mean ± SEM; *, $P < 0.05$. **B,** Mean tumor volume of subcutaneous 4T1 tumor in mice treated with control or 200 μg anti–PD-L1 antibody twice a week for 2 weeks in combination with 12.5 mg/kg BPTES or vehicle. **C** and **D,** The expression of ARG1 and Ly6G was detected in tumor tissues from control and anti–PD-L1-treated mice in combination with BPTES or vehicle (**C**). The number of positive cells is summarized in **D** ($n = 8$/group). Data from two independent experiments shown as mean ± SEM; **, $P < 0.01$. **E** and **F,** Representative flow-cytometric analysis and quantification of $CD8^+$ T cells (**E**); the frequency of $CD8^+$ T in total $CD45^+$ cells from 4T1 tumors (**F**) at 25 days after implantation ($n = 8$/group). **G** and **H,** Flow cytometry determined the proportion of $IFN\gamma^+$ and granzyme B^+ T cells in tumors from indicated groups (**G**). The percentage of $IFN\gamma^+$ and granzyme B^+ T cells is summarized in **H** ($n = 8$/group). Data from two independent experiments shown as mean ± SEM; *, $P < 0.05$; **, $P < 0.01$. The statistical significance of differences between groups was determined by a two-tailed Student *t* test.

metabolism of rapidly dividing cells has been identified (46, 47). However, we found that although glutamine-derived αKG supports the expansion of IMCs, αKG only partially rescues the suppressive marker of IMCs in glutamine-deprived conditions. These data strongly suggest that other component(s) from glutamine metabolism are involved in regulating the activation stage of IMC generation.

Studies indicate that metabolites, such as kynurenine, succinate, and lactate, can act as signaling molecules to induce trained immunity or suppressive function (48–50). Here, we found that glutamate, a metabolite from glutamine metabolism, was essential for regulating the activation of IMCs. Exogenous glutamate could either promote or restore M-CSFR expression on IMCs in normal or glutamine-deprived culture conditions. Accordingly, antagonism of the glutamate–NMDAR axis effectively blocked the activation of IMCs, but did not alter the cell number of IMCs. Importantly, the expression of an xCT antiporter, which transports glutamate out of the cells (42, 51), is significantly upregulated in tumors. The xCT antiporter is present primarily in the invasion margin of tumor tissues and is colocalized with suppressive myeloid cells.

Growing evidence has shown that metabolism can directly regulate immune cell function and responses to immune-checkpoint blockade treatment (19). Our results suggest that there are fine-tuned collaborative actions that regulate IMC differentiation in the TME. In glucose-limiting TME, the expansion of newly recruited myeloid progenitors is supported by glutamine-derived αKG. Glutamate, exported by tumor tissues, can further promote the activation of these cells to generate functional IMCs. Given the predominant role of suppressive myeloid cells in regulating immune responses in cancer, the present study provides important new insights into the mechanisms by which TME regulates the generation of IMCs. It is, therefore, reasonable to predict that selectively targeting TME and IMC differentiation might provide a novel strategy for immune-based anticancer therapies.

Disclosure of Potential Conflicts of Interest

No potential conflicts of interest were disclosed.

Authors' Contributions

Conception and design: H.-W. Sun, L. Zheng

Acquisition of data (provided animals, acquired and managed patients, provided facilities, etc.): W.-C. Wu, H.-W. Sun, J. Chen, H.-Y. OuYang, H.-T. Chen, Z.-Y. Shuang, M. Shi, Z. Wang

Analysis and interpretation of data (e.g., statistical analysis, biostatistics, computational analysis): W.-C. Wu, H.-W. Sun, J. Chen, L. Zheng

Writing, review, and/or revision of the manuscript: W.-C. Wu, H.-W. Sun, L. Zheng

Administrative, technical, or material support (i.e., reporting or organizing data, constructing databases): X.-J. Yu, H.-T. Chen, Z.-Y. Shuang, M. Shi, Z. Wang

Study supervision: L. Zheng

Acknowledgments

This work was supported by project grants from the National Key R&D Program of China (2017YFA0505803 and 2018ZX10302205), the National Natural Science Foundation of China (81502455, 81730044, 81802663, and 91842308), the Health Medical Collaborative Innovation Program of Guangzhou (201400000001–3), and the Fundamental Research Funds for the Central Universities (16lgjc46 and 171gjc32).

The costs of publication of this article were defrayed in part by the payment of page charges. This article must therefore be hereby marked *advertisement* in accordance with 18 U.S.C. Section 1734 solely to indicate this fact.

Received December 15, 2018; revised April 18, 2019; accepted July 31, 2019; published first August 6, 2019.

References

1. Engblom C, Pfirschke C, Pittet MJ. The role of myeloid cells in cancer therapies. Nat Rev Cancer 2016;16:447–62.
2. Gabrilovich DI, Nagaraj S. Myeloid-derived suppressor cells as regulators of the immune system. Nat Rev Immunol 2009;9:162–74.
3. Noy R, Pollard JW. Tumor-associated macrophages: from mechanisms to therapy. Immunity 2014;41:49–61.
4. Cui TX, Kryczek I, Zhao L, Zhao E, Kuick R, Roh MH, et al. Myeloid-derived suppressor cells enhance stemness of cancer cells by inducing microRNA101 and suppressing the corepressor CtBP2. Immunity 2013;39:611–21.
5. Condamine T, Ramachandran I, Youn JI, Gabrilovich DI. Regulation of tumor metastasis by myeloid-derived suppressor cells. Annu Rev Med 2015;66:97–110.
6. Di Mitri D, Toso A, Chen JJ, Sarti M, Pinton S, Jost TR, et al. Tumour-infiltrating Gr-1+ myeloid cells antagonize senescence in cancer. Nature 2014;515:134–7.
7. Liang H, Deng L, Hou Y, Meng X, Huang X, Rao E, et al. Host STING-dependent MDSC mobilization drives extrinsic radiation resistance. Nat Commun 2017;8:1736.
8. De Henau O, Rausch M, Winkler D, Campesato LF, Liu C, Cymerman DH, et al. Overcoming resistance to checkpoint blockade therapy by targeting PI3Kgamma in myeloid cells. Nature 2016;539:443–7.
9. Kumar V, Patel S, Tcyganov E, Gabrilovich DI. The nature of myeloid-derived suppressor cells in the tumor microenvironment. Trends Immunol 2016;37:208–20.
10. Lefrancais E, Ortiz-Munoz G, Caudrillier A, Mallavia B, Liu F, Sayah DM, et al. The lung is a site of platelet biogenesis and a reservoir for haematopoietic progenitors. Nature 2017;544:105–9.
11. Wu C, Ning H, Liu M, Lin J, Luo S, Zhu W, et al. Spleen mediates a distinct hematopoietic progenitor response supporting tumor-promoting myelopoiesis. J Clin Invest 2018;128:3425–38.
12. Ghesquiere B, Wong BW, Kuchnio A, Carmeliet P. Metabolism of stromal and immune cells in health and disease. Nature 2014;511:167–76.
13. Koziel A, Woyda-Ploszczyca A, Kicinska A, Jarmuszkiewicz W. The influence of high glucose on the aerobic metabolism of endothelial EA.hy926 cells. Pflugers Arch 2012;464:657–69.
14. Gerriets VA, Rathmell JC. Metabolic pathways in T cell fate and function. Trends Immunol 2012;33:168–73.
15. Galvan-Pena S, O'Neill LA. Metabolic reprograming in macrophage polarization. Front Immunol 2014;5:420.
16. Chen D, Xie J, Fiskesund R, Dong W, Liang X, Lv J, et al. Chloroquine modulates antitumor immune response by resetting tumor-associated macrophages toward M1 phenotype. Nat Commun 2018;9:873.
17. Biswas SK. Metabolic reprogramming of immune cells in cancer progression. Immunity 2015;43:435–49.
18. Siska PJ, Rathmell JC. T cell metabolic fitness in antitumor immunity. Trends Immunol 2015;36:257–64.
19. Chang CH, Qiu J, O'Sullivan D, Buck MD, Noguchi T, Curtis JD, et al. Metabolic competition in the tumor microenvironment is a driver of cancer progression. Cell 2015;162:1229–41.
20. Wang H, Franco F, Ho PC. Metabolic regulation of Tregs in cancer: opportunities for immunotherapy. Trends Cancer 2017;3:583–92.
21. O'Neill LA, Pearce EJ. Immunometabolism governs dendritic cell and macrophage function. J Exp Med 2016;213:15–23.

22. Michalek RD, Gerriets VA, Jacobs SR, Macintyre AN, MacIver NJ, Mason EF, et al. Cutting edge: distinct glycolytic and lipid oxidative metabolic programs are essential for effector and regulatory CD4+ T cell subsets. J Immunol 2011;186:3299–303.
23. Huang SC, Everts B, Ivanova Y, O'Sullivan D, Nascimento M, Smith AM, et al. Cell-intrinsic lysosomal lipolysis is essential for alternative activation of macrophages. Nat Immunol 2014;15:846–55.
24. Kuang DM, Xiao X, Zhao Q, Chen MM, Li XF, Liu RX, et al. B7-H1-expressing antigen-presenting cells mediate polarization of protumorigenic Th22 subsets. J Clin Invest 2014;124:4657–67.
25. Wu WC, Sun HW, Chen HT, Liang J, Yu XJ, Wu C, et al. Circulating hematopoietic stem and progenitor cells are myeloid-biased in cancer patients. Proc Natl Acad Sci U S A 2014;111:4221–6.
26. Morris KT, Khan H, Ahmad A, Weston LL, Nofchissey RA, Pinchuk IV, et al. G-CSF and G-CSFR are highly expressed in human gastric and colon cancers and promote carcinoma cell proliferation and migration. Br J Cancer 2014;110:1211–20.
27. Wang Y, Han G, Wang K, Liu G, Wang R, Xiao H, et al. Tumor-derived GM-CSF promotes inflammatory colon carcinogenesis via stimulating epithelial release of VEGF. Cancer Res 2014;74:716–26.
28. Bronte V, Brandau S, Chen SH, Colombo MP, Frey AB, Greten TF, et al. Recommendations for myeloid-derived suppressor cell nomenclature and characterization standards. Nat Commun 2016;7:12150.
29. Huang B, Pan PY, Li Q, Sato AI, Levy DE, Bromberg J, et al. Gr-1+CD115+ immature myeloid suppressor cells mediate the development of tumor-induced T regulatory cells and T-cell anergy in tumor-bearing host. Cancer Res 2006;66:1123–31.
30. Youn JI, Collazo M, Shalova IN, Biswas SK, Gabrilovich DI. Characterization of the nature of granulocytic myeloid-derived suppressor cells in tumor-bearing mice. J Leukoc Biol 2012;91:167–81.
31. Marigo I, Bosio E, Solito S, Mesa C, Fernandez A, Dolcetti L, et al. Tumor-induced tolerance and immune suppression depend on the C/EBPbeta transcription factor. Immunity 2010;32:790–802.
32. McCracken AN, Edinger AL. Nutrient transporters: the Achilles' heel of anabolism. Trends Endocrinol Metab 2013;24:200–8.
33. Moreadith RW, Lehninger AL. The pathways of glutamate and glutamine oxidation by tumor cell mitochondria. Role of mitochondrial NAD(P)+-dependent malic enzyme. J Biol Chem 1984; 259:6215–21.
34. Altman BJ, Stine ZE, Dang CV. From Krebs to clinic: glutamine metabolism to cancer therapy. Nat Rev Cancer 2016;16:619–34.
35. Lane AN, Fan TW. Regulation of mammalian nucleotide metabolism and biosynthesis. Nucleic Acids Res 2015;43:2466–85.
36. Metallo CM, Gameiro PA, Bell EL, Mattaini KR, Yang J, Hiller K, et al. Reductive glutamine metabolism by IDH1 mediates lipogenesis under hypoxia. Nature 2011;481:380–4.
37. Wise DR, Ward PS, Shay JE, Cross JR, Gruber JJ, Sachdeva UM, et al. Hypoxia promotes isocitrate dehydrogenase-dependent carboxylation of alpha-ketoglutarate to citrate to support cell growth and viability. Proc Natl Acad Sci U S A 2011;108:19611–6.
38. Sun RC, Denko NC. Hypoxic regulation of glutamine metabolism through HIF1 and SIAH2 supports lipid synthesis that is necessary for tumor growth. Cell Metab 2014;19:285–92.
39. Condamine T, Gabrilovich DI. Molecular mechanisms regulating myeloid-derived suppressor cell differentiation and function. Trends Immunol 2011;32:19–25.
40. Affaticati P, Mignen O, Jambou F, Potier MC, Klingel-Schmitt I, Degrouard J, et al. Sustained calcium signalling and caspase-3 activation involve NMDA receptors in thymocytes in contact with dendritic cells. Cell Death Differ 2011;18:99–108.
41. Kahlfuss S, Simma N, Mankiewicz J, Bose T, Lowinus T, Klein-Hessling S, et al. Immunosuppression by N-methyl-D-aspartate receptor antagonists is mediated through inhibition of Kv1.3 and KCa3.1 channels in T cells. Mol Cell Biol 2014;34:820–31.
42. Briggs KJ, Koivunen P, Cao S, Backus KM, Olenchock BA, Patel H, et al. Paracrine induction of HIF by glutamate in breast cancer: EglN1 senses cysteine. Cell 2016;166:126–39.
43. Hanahan D, Weinberg RA. Hallmarks of cancer: the next generation. Cell 2011;144:646–74.
44. Tardito S, Oudin A, Ahmed SU, Fack F, Keunen O, Zheng L, et al. Glutamine synthetase activity fuels nucleotide biosynthesis and supports growth of glutamine-restricted glioblastoma. Nat Cell Biol 2015;17:1556–68.
45. DeBerardinis RJ, Cheng T. Q's next: the diverse functions of glutamine in metabolism, cell biology and cancer. Oncogene 2010;29:313–24.
46. Coloff JL, Murphy JP, Braun CR, Harris IS, Shelton LM, Kami K, et al. Differential glutamate metabolism in proliferating and quiescent mammary epithelial cells. Cell Metab 2016;23:867–80.
47. TeSlaa T, Chaikovsky AC, Lipchina I, Escobar SL, Hochedlinger K, Huang J, et al. alpha-Ketoglutarate accelerates the initial differentiation of primed human pluripotent stem cells. Cell Metab 2016;24:485–93.
48. Liu Y, Liang X, Dong W, Fang Y, Lv J, Zhang T, et al. Tumor-repopulating cells induce PD-1 expression in CD8(+) T cells by transferring kynurenine and AhR activation. Cancer Cell 2018;33:480–94.
49. Lee DC, Sohn HA, Park ZY, Oh S, Kang YK, Lee KM, et al. A lactate-induced response to hypoxia. Cell 2015;161:595–609.
50. Tannahill GM, Curtis AM, Adamik J, Palsson-McDermott EM, McGettrick AF, Goel G, et al. Succinate is an inflammatory signal that induces IL-1beta through HIF-1alpha. Nature 2013;496:238–42.
51. Timmerman LA, Holton T, Yuneva M, Louie RJ, Padro M, Daemen A, et al. Glutamine sensitivity analysis identifies the xCT antiporter as a common triple-negative breast tumor therapeutic target. Cancer Cell 2013;24: 450–65.